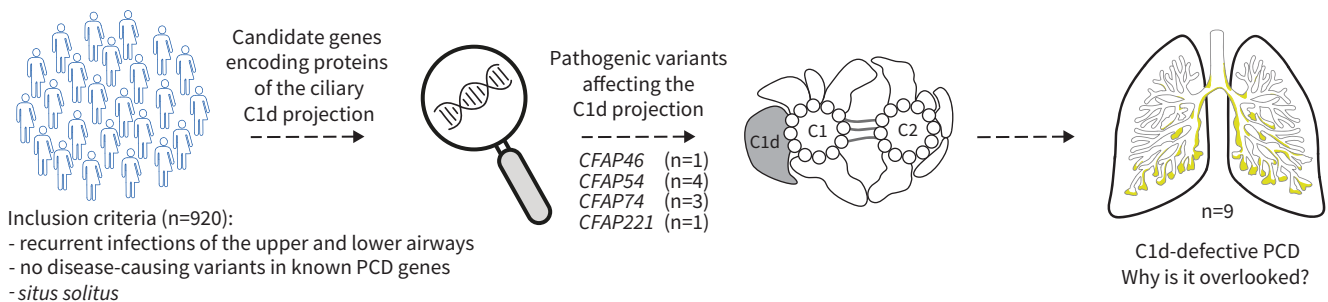


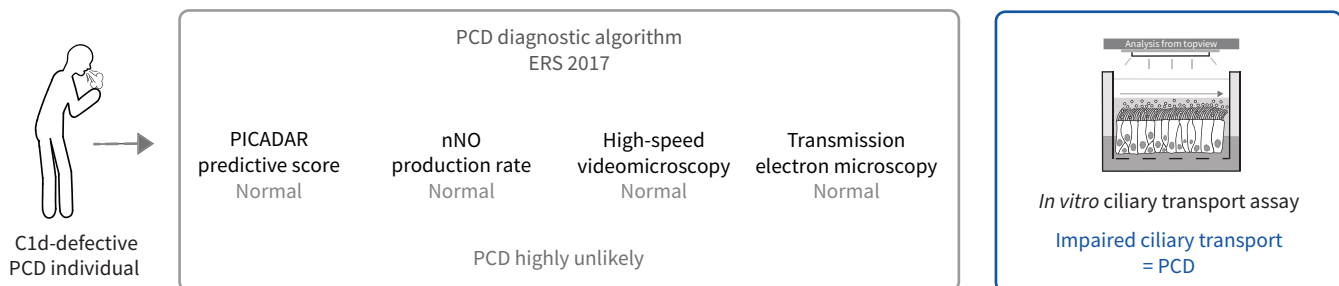
Pathogenic variants in *CFAP46*, *CFAP54*, *CFAP74* and *CFAP221* cause primary ciliary dyskinesia with a defective C1d projection of the central apparatus

Kai Wohlgemuth, Niklas Hoersting , Julia Koenig , Niki Tomas Loges, Johanna Raidt, Sebastian George, Sandra Cindrić, Andre Schramm, Luisa Biebach, Simon Lay, Gerard W. Dougherty, Heike Olbrich, Petra Pennekamp, Bernd Dworniczak and Heymut Omran

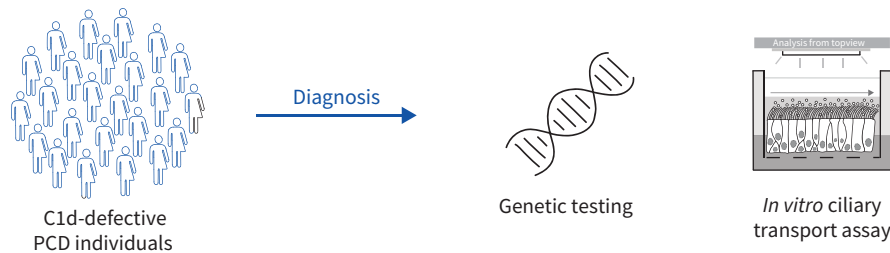
Aim and methods



Clinical and diagnostic findings






Conclusion



GRAPHICAL ABSTRACT In this study, we examined a cohort of individuals exhibiting recurrent upper and lower airway infections combined with situs solitus (n=920) who had not received a diagnosis previously. Using a high-throughput sequencing approach of genes encoding components of the C1d projection of the central apparatus, we identified pathogenic variants in *CFAP46*, *CFAP54*, *CFAP74* and *CFAP221* as a cause of C1d-defective primary ciliary dyskinesia (PCD) (n=9). Affected individuals easily elude the current European Respiratory Society (ERS) diagnostic algorithm because this PCD type is associated with normal findings on PICADAR, nasal nitric oxide (nNO) production rate, high-speed videomicroscopy and transmission electron microscopy. However, C1d-defective PCD individuals exhibit impaired ciliary transport. In conclusion, only genetic testing and *in vitro* ciliary transport assays enable diagnosis of C1d-defective PCD.



Pathogenic variants in *CFAP46*, *CFAP54*, *CFAP74* and *CFAP221* cause primary ciliary dyskinesia with a defective C1d projection of the central apparatus

Kai Wohlgemuth^{1,3}, Niklas Hoersting ^{1,3}, Julia Koenig ¹, Niki Tomas Loges¹, Johanna Raidt¹, Sebastian George¹, Sandra Cindrić¹, Andre Schramm¹, Luisa Biebach¹, Simon Lay², Gerard W. Dougherty¹, Heike Olbrich¹, Petra Pennekamp¹, Bernd Dworniczak¹ and Heymut Omran ¹

¹Department of General Pediatrics, University Children's Hospital Muenster, Muenster, Germany. ²Department of Pediatric Pneumology and Allergology, Fachkliniken Wangen, Wangen, Germany. ³These authors contributed equally to this work.

Corresponding author: Heymut Omran (heymut.omran@ukmuenster.de)



Shareable abstract (@ERSpublications)

Pathogenic variants in *CFAP46*, *CFAP54*, *CFAP74* and *CFAP221* cause C1d-defective PCD with normal body laterality, nasal NO production, ciliary ultrastructure and ciliary beating. Only genetic testing and ciliary transport assays enable reliable diagnosis. <https://bit.ly/3XkHJ4n>

Cite this article as: Wohlgemuth K, Hoersting N, Koenig J, *et al.* Pathogenic variants in *CFAP46*, *CFAP54*, *CFAP74* and *CFAP221* cause primary ciliary dyskinesia with a defective C1d projection of the central apparatus. *Eur Respir J* 2024; 64: 2400790 [DOI: 10.1183/13993003.00790-2024].

Copyright ©The authors 2024.

This version is distributed under the terms of the Creative Commons Attribution Non-Commercial Licence 4.0. For commercial reproduction rights and permissions contact permissions@ersnet.org

This article has an editorial commentary:
<https://doi.org/10.1183/13993003.01888-2024>

Received: 25 April 2024
Accepted: 22 Aug 2024

Abstract

Background Primary ciliary dyskinesia is a rare genetic disorder caused by insufficient mucociliary clearance leading to chronic airway infections. The diagnostic guideline of the European Respiratory Society primarily recommends an evaluation of the clinical history (*e.g.* by the PICADAR prediction tool), nasal nitric oxide production rate measurements, high-speed videomicroscopy analysis of ciliary beating and an assessment of ciliary axonemes *via* transmission electron microscopy. Genetic testing can be implemented as a last step.

Aims In this study, we aimed to characterise primary ciliary dyskinesia with a defective C1d projection of the ciliary central apparatus and we evaluated the applicability of the European Respiratory Society diagnostic guideline to this primary ciliary dyskinesia type.

Methods Using a high-throughput sequencing approach of genes encoding C1d components, we identified pathogenic variants in the novel primary ciliary dyskinesia genes *CFAP46* and *CFAP54*, and the known primary ciliary dyskinesia gene *CFAP221*. To fully assess this primary ciliary dyskinesia type, we also analysed individuals with pathogenic variants in *CFAP74*.

Results Careful evaluation revealed that C1d-defective primary ciliary dyskinesia is associated with normal situs composition, normal nasal nitric oxide production rates, normal ciliary ultrastructure by transmission electron microscopy and normal ciliary beating by high-speed videomicroscopy analysis. Despite chronic respiratory disease, PICADAR does not reliably detect this primary ciliary dyskinesia type. However, we could show by *in vitro* ciliary transport assays that affected individuals exhibit insufficient ciliary clearance.

Conclusions Overall, this study extends the spectrum of primary ciliary dyskinesia genes and highlights that individuals with C1d-defective primary ciliary dyskinesia elude diagnosis when using the current diagnostic algorithm. To enable diagnosis, genetic testing should be prioritised in future diagnostic guidelines.

Introduction

Primary ciliary dyskinesia (PCD) (OMIM24440) is a rare genetic disorder caused by dysfunctional motile cilia lining the surface of the airways (figure 1a). Impaired mucociliary clearance leads to chronic respiratory tract infections, including chronic wet cough, bronchitis, rhinosinusitis, recurrent otitis media, mucostasis and bronchiectasis [1, 2]. To date, variants in over 50 genes have been reported to cause PCD, recently estimated to affect at least one in 8000 individuals [3].



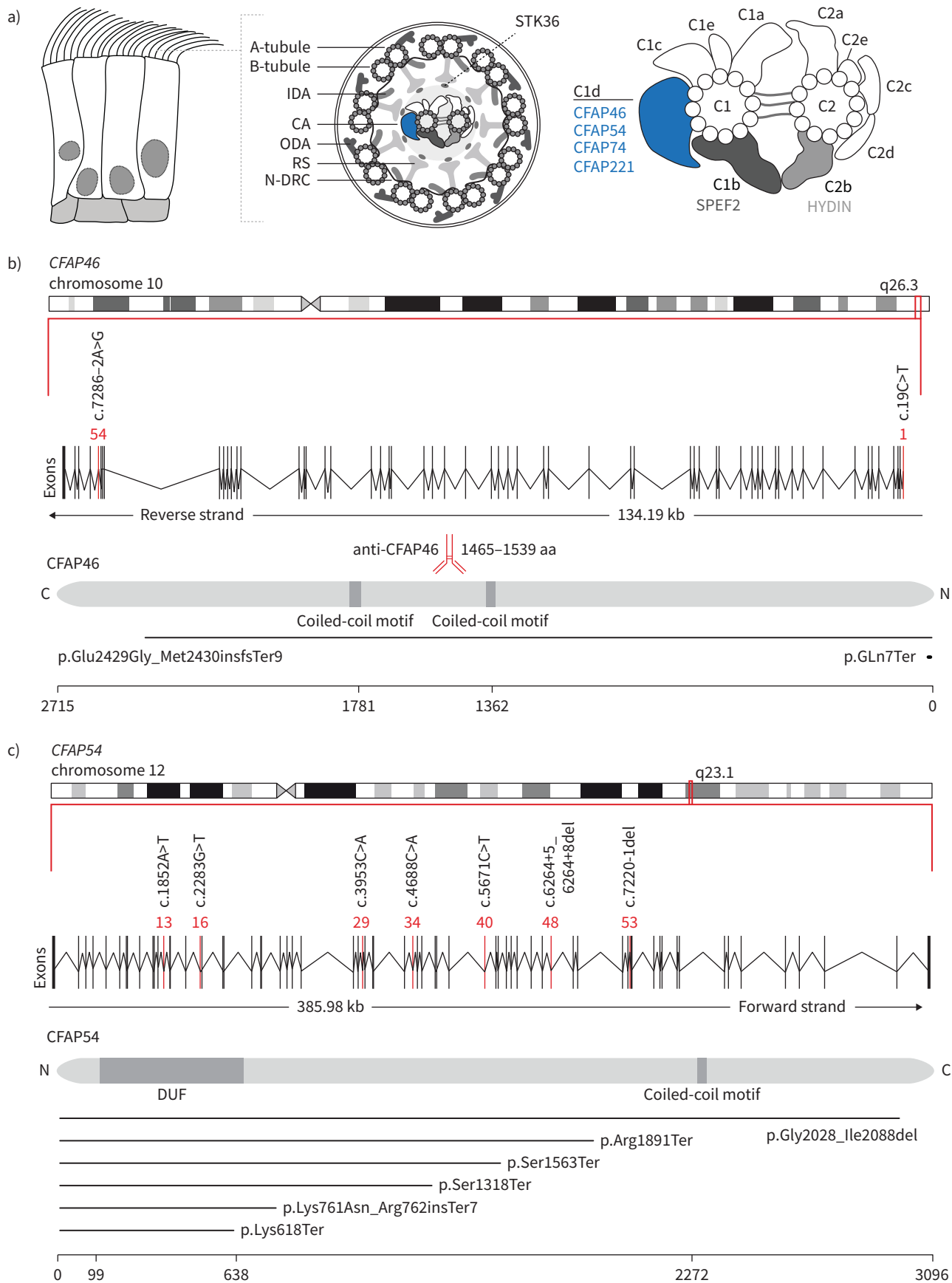


FIGURE 1 Pathogenic variants in *CFAP46* and *CFAP54* cause primary ciliary dyskinesia with a defective C1d projection. **a)** Schematic of respiratory epithelium (left), an axonemal 9+2 cross-section (middle) and the ciliary central apparatus (CA) (right). *CFAP46*, *CFAP54*, *CFAP74* and *CFAP221* localise to the C1d projection of the CA. *SPEF2* is part of the C1b projection, *HYDIN* of the C2b projection; *STK36* is predicted to localise between the CA and radial spoke (RS). IDA: inner dynein arm; ODA: outer dynein arm; N-DRC: nexin-dynein regulatory complex. **b)** *CFAP46* is located on chromosome 10 and encodes a 2715 amino acid (aa) protein with two coiled-coil motifs. The epitope of the anti-*CFAP46* antibody is located between the two coiled-coil motifs and specifically recognises *CFAP46*. The positions of the identified pathogenic variants in *CFAP46* are indicated by exons highlighted in red. Resulting truncated proteins are indicated below. **c)** *CFAP54* is located on chromosome 12 and encodes a 3096 aa protein with a domain of unknown function (DUF) and a coiled-coil motif. The positions of the identified pathogenic variants in *CFAP54* are indicated by exons highlighted in red. Resulting truncated proteins are indicated below.

The ciliary axoneme comprises nine outer microtubule doublets and distinct multiprotein complexes such as outer dynein arms, nexin-dynein regulatory complexes and radial spokes surrounding the central apparatus (CA). The CA consists of a central pair of single microtubules (9+2) with associated multiprotein projections (figure 1a) [1, 4]. In humans, the role of individual CA components in the regulation of ciliary beating and its impact on disease burden are still poorly understood and current knowledge is mainly based on findings in model organisms such as *Chlamydomonas reinhardtii* [5]. In this unicellular green alga, 11 projections are linked to the CA. Six of them attach to the C1 microtubule (C1a, C1b, C1c, C1d, C1e, C1f) and five attach to the C2 microtubule (C2a, C2b, C2c, C2d, C2e). In mammals, the C1f projection is absent (figure 1a) [6].

Owing to the complexity of PCD, it is not possible to diagnose all types of PCD with a single test. Therefore, the current European Respiratory Society (ERS) diagnostic guideline recommends the sequential performance of several different tests (supplementary figure S1) [7]. Accordingly, an evaluation of the clinical history is recommended, for which the calculation of the anamnesis-based PICADAR score is suggested (maximum score 14) [7, 8]. Subsequently, nasal NO (nNO) production rate measurements (cut-off $<77 \text{ nL} \cdot \text{min}^{-1}$) and high-speed videomicroscopy analysis (HSVMA) to evaluate ciliary beating immediately after sampling should be performed. In individuals with low nNO production rates, abnormal HSVMA or a clinically high suspicion of PCD, transmission electron microscopy (TEM) of ciliary axonemes and HSVMA after air-liquid interface (ALI) culture should be performed to differentiate PCD from secondary dyskinesia. In case of normal test results but a very strong clinical history suggestive for PCD, genetic testing can be implemented [7].

PCD individuals with a defective CA display normal ciliary ultrastructure on TEM. In addition, affected individuals exhibit situs solitus because the embryonic nodal 9+0 cilia influencing organ positioning lack the CA [9–13]. So far, we have identified PCD-causing variants in *SPEF2* and *HYDIN*, encoding large proteins of the C1b and C2b projection, respectively [9, 11]. We have also reported *STK36* as a PCD gene encoding an axonemal component, possibly intercalating the radial spoke heads with the CA (figure 1a) [10]. Recently, we and others identified PCD-causing variants in *CFAP74* and *CFAP221*, encoding components of the C1d projection [12–14]. In addition, there was a report of two individuals with pathogenic variants in *CFAP54*, a gene also encoding a C1d component [15]. However, no confirmative test documenting abnormal ciliary function has been reported in these individuals. Thus, it remains unclear whether pathogenic *CFAP54* variants indeed result in PCD.

In this study, we aimed to better characterise PCD with a defective C1d projection. Using next-generation sequencing, we investigated a large cohort of PCD-suspected individuals (n=920) for variants in known PCD genes (*CFAP74*, *CFAP221*) and candidate genes (*CFAP46*, *CFAP54*, *CFAP99*, *CFAP297*), all encoding C1d components. Inclusion criteria were recurrent airway infections typical for PCD and the presence of situs solitus. Moreover, the study individuals had not previously received an adequate diagnosis and did not have disease-causing variants in other known PCD genes (supplementary table S1).

With this strategy, we identified six affected individuals with unreported pathogenic variants in the novel PCD genes *CFAP46* and *CFAP54* (figure 1b, c and figure 2) and the known PCD gene *CFAP221* (supplementary figure S2). Recently, we identified pathogenic *CFAP74* variants as a cause of PCD in three individuals, providing the opportunity to study C1d-defective PCD in a total of nine individuals [13]. Careful assessment revealed that this PCD type is associated with normal findings regarding PICADAR scores, nNO production rates, ciliary ultrastructure and ciliary beating. However, affected individuals exhibit insufficient ciliary clearance as demonstrated by *in vitro* ciliary transport assays. This is consistent with chronic respiratory disease, underlining the importance of identifying affected individuals.

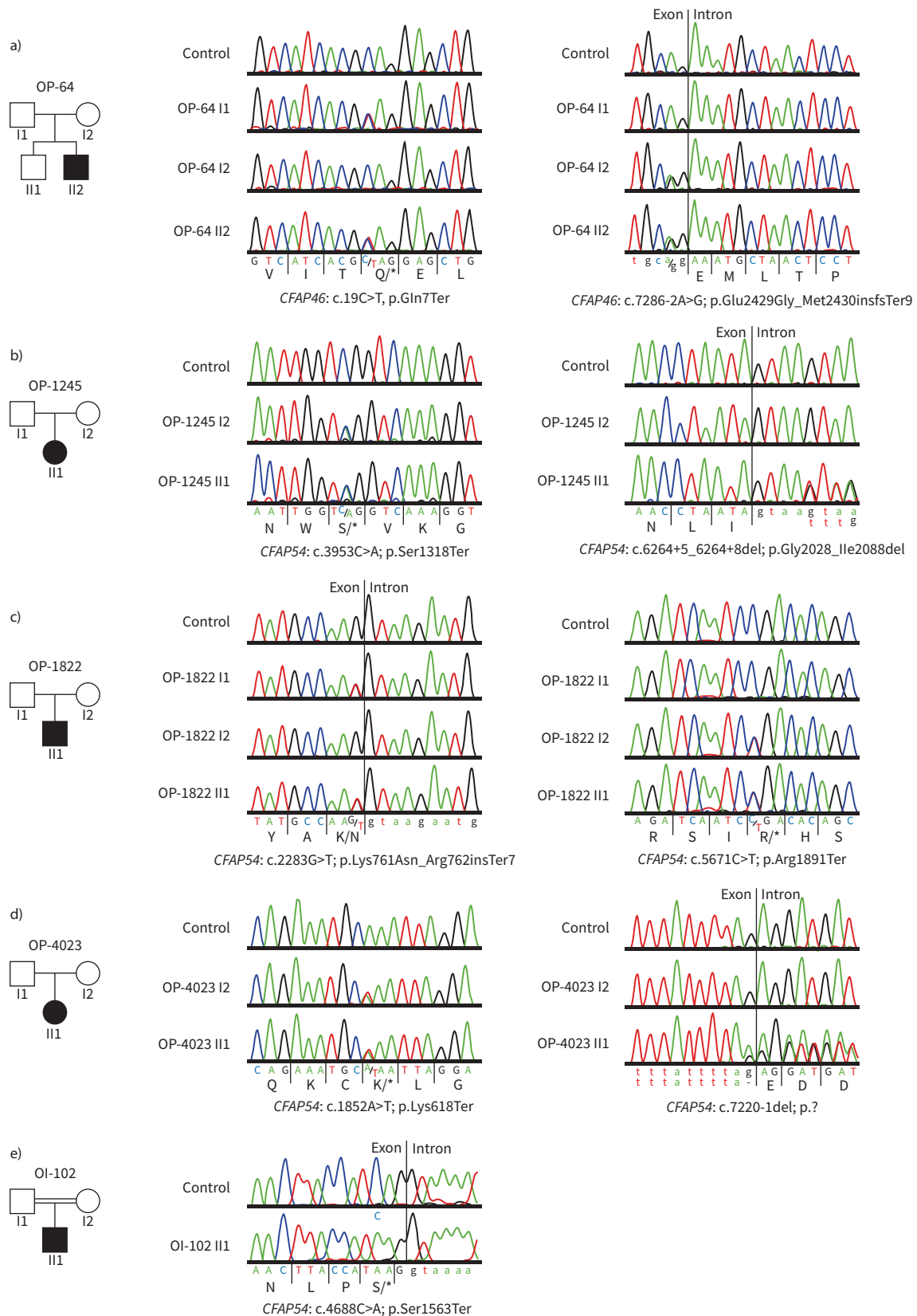


FIGURE 2 Sanger verification and segregation analysis of primary ciliary dyskinesia individuals harbouring biallelic pathogenic variants in *CFAP46* and *CFAP54*. a–e) Pedigrees of the five families are indicated. Sanger sequencing confirms compound heterozygosity of the detected variants in OP-64 II2 (a), OP-1245 II1 (b), OP-1822 II1 (c) and OP-4023 II1 (d). OI-102 II1 shows a homozygous variant consistent with homozygosity by descent due to parental consanguinity (e).

Materials and methods

Study population

Using next-generation sequencing, we investigated a large cohort of 920 PCD-suspected individuals for variants in known PCD genes (*CFAP74*, *CFAP221*) and candidate genes (*CFAP46*, *CFAP54*, *CFAP99*, *CFAP297*), all encoding C1d components. The main inclusion criteria for this cohort were recurrent airway infections and the presence of situs solitus.

Genetic testing

Genomic DNA was isolated directly from blood using standard methods. High-throughput sequencing was performed including whole exome sequencing, whole genome sequencing and a customised PCD gene panel [11, 16, 17], comprising the genes *CFAP46*, *CFAP54*, *CFAP74*, *CFAP221*, *CFAP99* and *CFAP297*. The pathogenicity of identified variants was assessed according to the consensus recommendation of the American College of Medical Genetics and Genomics (ACMG) [18]. Minor allele frequencies (MAFs) were obtained from GnomAD (<https://gnomad.broadinstitute.org/>), and variants affecting the splice site were verified using varSEAK (www.varSEAK.bio).

Culture of respiratory epithelial cells

Human respiratory epithelial cells were obtained by nasal brush biopsy from healthy control individuals and the affected individuals OP-64 II2, OP-1245 II1 and OP-1822 II2 and were cultured at the ALI as described previously [19].

High-speed videomicroscopy analysis

HSVMA was performed in native and ALI-cultured respiratory epithelial cells. The evaluation of ciliary beat frequency (CBF) and pattern was performed as described by RAJDT *et al.* [20].

Nasal nitric oxide production rate measurements

Measurements of the nNO production rates ($\text{nL} \cdot \text{min}^{-1}$) were performed as previously described [21].

Transmission electron microscopy

TEM was performed with freshly obtained respiratory epithelial cells (OP-2697 I2) or after ALI culture (OP-64 II2, OP-1245 II1, OP-1822 II1) as previously reported [19].

High-resolution immunofluorescence microscopy

For high-resolution immunofluorescence (IF) microscopy, respiratory epithelial cell samples were recovered by nasal brush biopsies from affected individuals. The samples were treated and incubated with primary and secondary antibodies as described by OMRAN and LOGES [22].

Protein extraction and immunoblot analyses

Fully differentiated ALI-cultured respiratory epithelial cells from OP-64 II2 and a healthy control individual were used for the preparation of extracts enriched for axonemal and cytoplasmic proteins as previously described [11, 17]. Immunoblotting was performed as reported [17].

In vitro ciliary transport assays

In vitro ciliary transport assays evaluate the transport of fluorescent particles by ciliary beating on ALI-cultured respiratory epithelium from the top view [17]. Cells from OP-64 II2, OP-1245 II1 and OP-1822 II1 were available for analyses. Analyses were performed on a Leica Thunder Imager (OP-64 II2, OP-1245 II1) or Nikon Eclipse Ti-S phase-contrast microscope (OP-1822 II1). The significance levels were calculated using a t-test. A p-value ≤ 0.05 was considered significant.

A detailed description of the materials and methods is provided in the supplementary material.

Results

Genetic findings

In five affected individuals from five unrelated families, we identified novel pathogenic variants in *CFAP46* and *CFAP54* according to ACMG criteria (figures 1 and 2) [18].

In the 22-year-old male individual OP-64 II2 from a non-consanguineous German family, we detected the pathogenic heterozygous *CFAP46* (NM_001200049.3) nonsense variant c.19C>T, p.Gln7Ter (MAF: 2.59×10^{-3}) and the pathogenic heterozygous splice-site variant c.7286-2A>G, p.Glu2429Gly_Met2430insfsTer9 (MAF: 2.03×10^{-3} , varSEAK: class 5) (figure 1b). Segregation analysis verified compound heterozygosity by detecting the heterozygous variant c.19C>T in the father and the heterozygous variant c.7286-2A>G in the mother

(figure 2a). Complementary DNA (cDNA) sequencing revealed that c.7286-2A>G leads to activation of a cryptic splice site, causing a frameshift and premature stop of translation (p.Glu2429Gly_Met2430insfsTer9) and resulting in a truncation of CFAP46 (figure 1b and supplementary figure S3a, b).

In four other individuals (OP-1245 II1, OP-1822 II1, OP-4023 II1, OI-102 II1), we identified pathogenic *CFAP54* (NM_001306084.2) variants. The 25-year-old female individual OP-1245 II1, originating from a non-consanguineous German family, carried the pathogenic heterozygous *CFAP54* nonsense variant c.3953C>A, p.Ser1318Ter (not listed in GnomAD database) and the pathogenic heterozygous splice-site variant c.6264+5_6264+8del, p.Gly2028_Ile2088del (MAF: $9.34e^{-06}$, varSEAK: class 5) (figure 1c). Consistent with compound heterozygosity, segregation analysis confirmed the heterozygous variant c.3953C>A in the mother (figure 2b). Paternal DNA was not available. cDNA sequencing demonstrated that c.6264+5_6264+8del causes skipping of exon 44, resulting in an in-frame deletion (supplementary figure S4a, b).

We further identified the pathogenic heterozygous *CFAP54* nonsense variant c.2283G>T, p.Lys761Asn_Arg762insTer7 (MAF: $6.58e^{-06}$) and pathogenic heterozygous nonsense variant c.5671C>T, p.Arg1891Ter (MAF: $1.6e^{-05}$) in the 16-year-old male individual OP-1822 II1 from a non-consanguineous German family (figure 1c). Segregation analyses confirmed the heterozygous variant c.2283G>T in the father and the heterozygous variant c.5671C>T in the mother, demonstrating compound heterozygosity (figure 2c). Because c.2283G>T affects the boundary of exon-intron 16, we performed cDNA analysis, revealing aberrant splicing for this variant and a retention of intron 16, resulting in a frameshift and premature stop of translation (supplementary figure S4c, d).

In the 2-year-old female individual OP-4023 II1 descended from a non-consanguineous German family, we detected the pathogenic heterozygous *CFAP54* nonsense variant c.1852A>T, p.Lys618Ter (MAF: $2.39e^{-04}$) and pathogenic heterozygous splice-site variant c.7220-1del, p.? (not listed in GnomAD database, varSEAK: class 5) (figure 1c). Segregation analysis confirmed the heterozygous variant c.1852A>T in the mother, consistent with compound heterozygosity (figure 2d). Paternal DNA was not available.

In the 22-year-old male individual OI-102 II1 from a consanguineous Israeli family, we identified the pathogenic homozygous *CFAP54* nonsense variant c.4688C>A, p.Ser1563Ter (not listed in GnomAD database) (figures 1c and 2e).

Recently, we reported pathogenic variants in *CFAP74* (NM_001304360.2) as a cause of PCD [13]. In two adult siblings from a non-consanguineous German family (OP-3882 II1 and OP-3882 II2), we detected the pathogenic compound-heterozygous *CFAP74* variants c.907del, p.Gln303LysfsTer65 and c.4380_4381dup, p.Phe1461SerfsTer12 (table 1). OP-4027 II1, a 14-year-old male individual from a non-consanguineous German family, carries the pathogenic compound-heterozygous *CFAP74* variants c.4380_4381dup, p.Phe1461SerfsTer12 and c.1706dup, p.Gly570TrpfsTer10 [13].

Recently, *CFAP221* (NM_001271049.2) variants have been published as cause of PCD [12]. We identified the unreported pathogenic homozygous *CFAP221* frameshift variant c.1641dup, p.Asn548GlnfsTer6 (MAF: $1.2e^{-04}$) in the 39-year-old female individual OP-2697 I2, consistent with homozygosity by descent due to parental consanguinity (table 1).

Clinical findings

The C1d-defective PCD individuals with pathogenic variants in the novel PCD genes *CFAP46* and *CFAP54* and the known PCD genes *CFAP74* and *CFAP221* all exhibited chronic respiratory disease, including mucus plugging and bronchiectasis (table 1). OP-64 II2 (*CFAP46*) had been hospitalised on several occasions owing to recurrent respiratory infections. Since early infancy, he reported wet cough, bronchitis, chronic rhinosinusitis, otitis media and recurrent pneumonia. Computed tomography (CT) and magnetic resonance imaging (MRI) of the lower and upper airways displayed situs solitus, mucus plugging, mild bronchiectasis in the lower lobes and polyposis nasi with mucosal thickening (table 1 and figure 3a). Spermogram of OP-64 II2 (*CFAP46*) showed normal results, which does not completely rule out subtle swimming deficits (supplementary table S2). The PICADAR indicated a score of 4 (table 1) and the nNO production rate was $235.6 \text{ nL} \cdot \text{min}^{-1}$. OP-1245 II1 (*CFAP54*) reported chronic wet cough, rhinosinusitis and recurrent pneumonia. CT and MRI scans showed situs solitus, mucus plugging, mild bronchiectasis, agenesis of frontal sinuses and mucosal thickening (figure 3b). The PICADAR yielded a score of 3 (table 1) and the nNO production rate was $182.3 \text{ nL} \cdot \text{min}^{-1}$. OP-1822 II1 (*CFAP54*) reported a period of neonatal respiratory distress including pneumonia and admission to neonatal intensive care. He had chronic bronchitis. Beside situs solitus, the patient displayed mucus plugging, dystelectasis and mild

TABLE 1 Genetic and clinical findings in C1d-defective PCD individuals

Individual	Genetics		Clinical data													PICADAR				
	Allele 1	Allele 2	Cons.	Gender	AAD (years)	Situs	nNO (nL·min ⁻¹)	HSVMA (native)	HSVMA (after ALI)	TEM	CRD	Bx/MP	FT gest. =2	NCS =2	NICU =2	Situs abn. =4	CHD =2	CR =1	CEHS =1	Total
CFAP46																				
NM_001200049.3																				
OP-64 II2	c.19C>T, p.Gln7Ter	c.7286-2A>G, p.Glu2429Gly_Met2430insfsTer9	No	M	23	Solitus	235.6	Normal	Normal	Normal	Yes	Yes	Yes	No	No	No	No	Yes	Yes	4
CFAP54																				
NM_00000524981.9																				
OI-102 II1	c.4688C>A, p.Ser1563Ter	c.4688C>A, p.Ser1563Ter	Yes	M	22	Solitus	NA	NA	NA	NA	Yes	Yes	NA	NA	NA	no	NA	NA	NA	NA
OP-1245 II1	c.3953C>A, p.Ser1318Ter	c.6264+5_6264+8del, p.Gly2028_1le2088del	No	F	25	Solitus	182.3	Normal	Normal	Normal	Yes	Yes	Yes	No	No	No	No	Yes	No	3
OP-1822 II1	c.2283G>T, p.Lys761Asn_Arg762insTer7	c.5671C>T, p.Arg1891Ter	No	M	16	Solitus	176.4	Normal	Normal	Normal	Yes	Yes	Yes	Yes	Yes	No	No	No	No	6
OP-4023 II1	c.1852A>T, p.Lys618Ter	c.7220-1delG, p.?	No	F	2	Solitus	NA	Normal	NA	NA	Yes	NA	Yes	Yes	Yes	No	No	Yes	No	7
CFAP74																				
NM_001304360.2																				
OP-3882 II1	c.907del, p.Gln303LysfsTer65	c.4380_4381dup, p.Phe1461SerfsTer12	No	M	48	Solitus	NA	NA	Normal	Normal	Yes	Yes	Yes	No	No	No	No	No	No	2
OP-3882 II2	c.907del, p.Gln303LysfsTer65	c.4380_4381dup, p.Phe1461SerfsTer12	No	F	57	Solitus	251.5	Normal	Normal	Normal	Yes	Yes	Yes	No	No	No	No	No	No	2
OP-4027 II1	c.1706dup, p.Gly570TrpfsTer10	c.4380_4381dup, p.Phe1461SerfsTer12	No	M	14	Solitus	504.6	Normal	NA	NA	Yes	NA	Yes	No	No	No	No	Yes	No	3
CFAP221																				
NM_001271049.2																				
OP-2697 I2	c.1641dup, p.Asn548GlnfsTer6	c.1641dup, p.Asn548GlnfsTer6	Yes	F	39	Solitus	28.9	Normal	NA	Normal	Yes	Yes	Yes	No	No	No	No	Yes	Yes	4

Genetic and clinical data of PCD individuals with pathogenic variants in *CFAP46*, *CFAP54*, *CFAP74* and *CFAP221*. The parameters of PICADAR are applied to the identified C1d-defective PCD individuals. The total scores result from the addition of the respective points and correspond to the following probabilities of having PCD: 2=0.8%; 3=1.9%; 4=4.7%; 6=23.9%; 7=44.1%. The maximum score is 14 [8]. PCD: primary ciliary dyskinesia; Cons.: consanguinity; AAD: age at diagnosis; nNO: nasal nitric oxide production rate; HSVMA: high-speed videomicroscopy analysis; ALI: air-liquid interface; TEM: transmission electron microscopy; CRD: chronic respiratory disease; Bx/MP: bronchiectasis/mucus plugging; FT gest.: full-term gestation; NCS: neonatal chest symptoms; NICU: neonatal intensive care admittance; Situs abn.: situs abnormalities; CHD: congenital heart defect; CR: chronic rhinitis; CEHS: chronic ear and hearing symptoms; M: male; NA: not available; F: female.

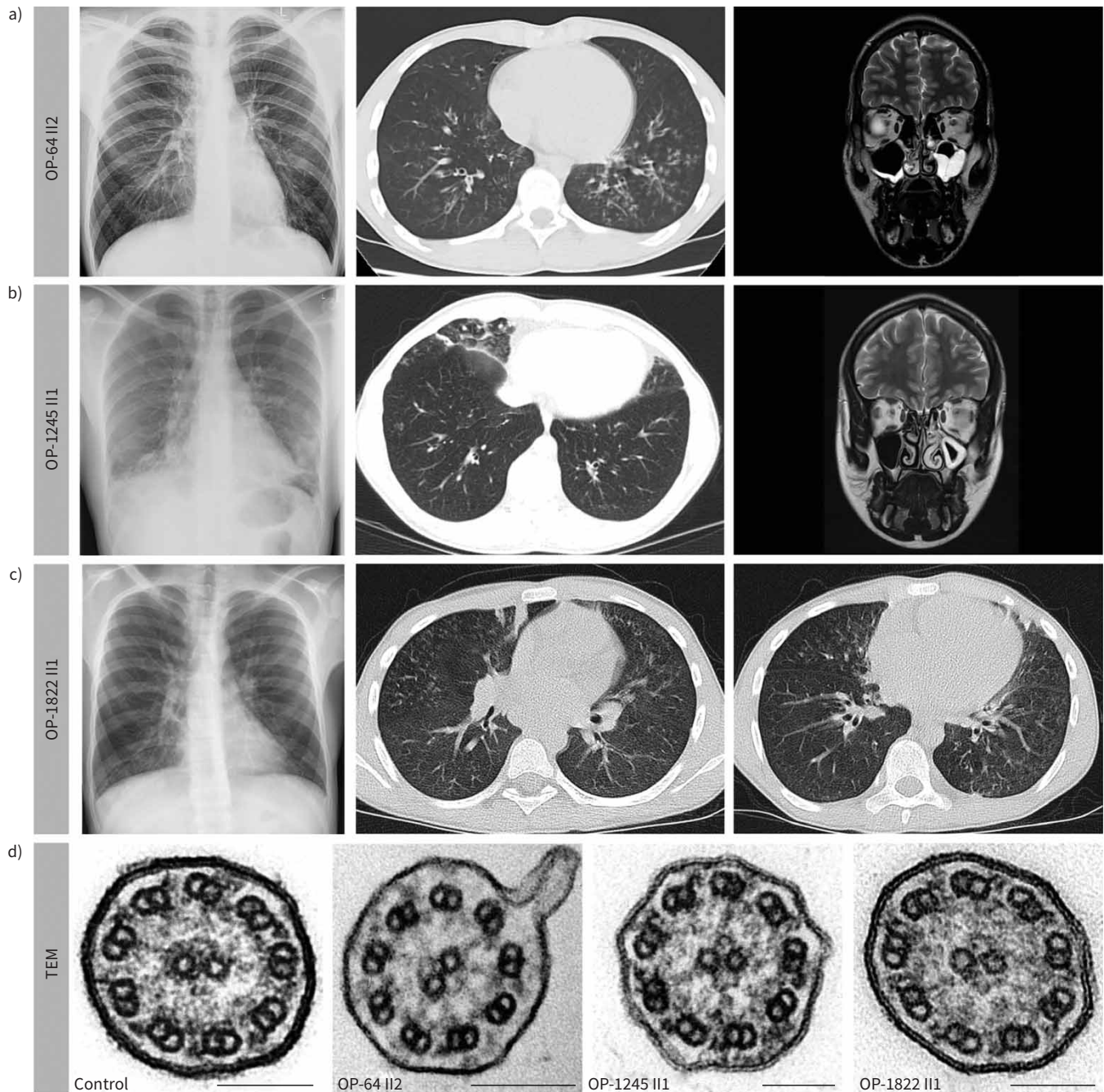


FIGURE 3 Radiological and ultrastructural findings in primary ciliary dyskinesia individuals with biallelic pathogenic *CFAP46* and *CFAP54* variants. **a)** *CFAP46*-variant individual OP-64 II2 shows situs solitus, mucus plugging and bronchiectasis in the lower lobes on chest X-ray (left panel) and computed tomography (CT) (middle panel). Consistent with chronic rhinosinusitis, magnetic resonance imaging (MRI) (right panel) displays mucosal thickening mainly in the left maxillary sinus and left ethmoidal cells, nasal mucosa swelling and nasal polyps. **b)** *CFAP54*-variant individual OP-1245 III exhibits situs solitus, basal lung consolidations, mucus plugging and mild bronchiectasis in the middle and lower lobes as well as in the lingula (chest X-ray: left panel; CT: middle panel). MRI scan (right panel) shows swelling of nasal mucosa and mucosal thickening in the left maxillary sinus and ethmoidal cells. Left ethmoidal infundibulum is blocked. **c)** *CFAP54*-variant individual OP-1822 III displays situs solitus, mucus plugging, dystelectasis and bronchiectasis in the lower lobes (chest X-ray: left panel; CT: right and middle panels). **d)** All individuals (OP-64 II2, OP-1245 III and OP-1822 III) show normal ciliary ultrastructure in transmission electron microscopy. Scale bars: 100 nm.

bronchiectasis in the lower lobes (figure 3c). The PICADAR score was 6 (table 1). The nNO production rate was $176.4 \text{ nL} \cdot \text{min}^{-1}$. OP-4023 III (*CFAP54*) had situs solitus, chronic wet cough, bronchitis and rhinitis and was admitted to neonatal intensive care due to neonatal respiratory distress. The PICADAR

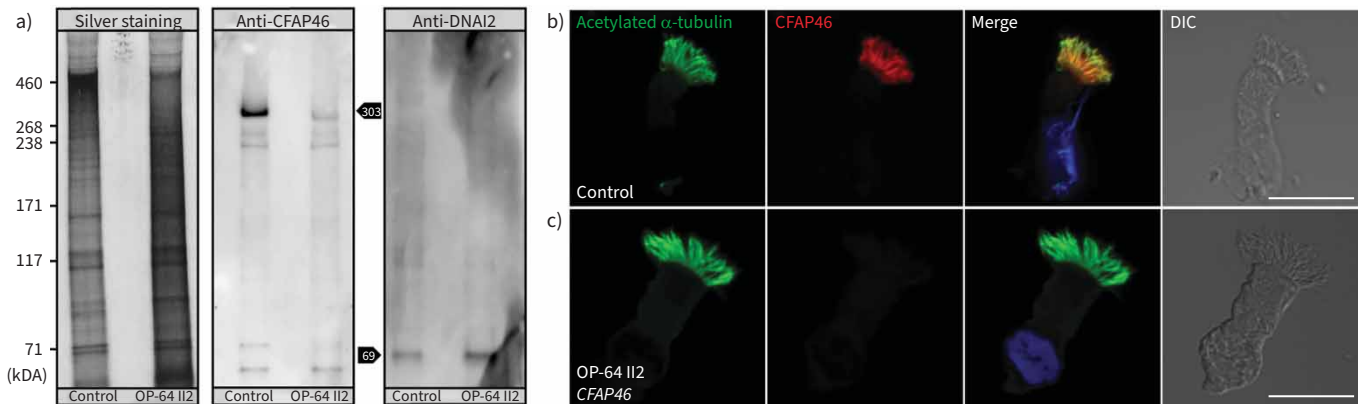


FIGURE 4 CFAP46 is undetectable in respiratory cilia from the CFAP46-variant individual OP-64 II2. **a)** Extracts enriched for axonemal proteins from air–liquid interface-cultured respiratory epithelial cells are used for silver staining and immunoblotting. Silver staining demonstrates the integrity of protein recovery after lithium dodecyl sulfate-polyacrylamide gel electrophoresis. Immunoblotting with anti-CFAP46 detects the 303 kDa large isoform of CFAP46 (Q8IYW2-1) in the axonemal extract from a healthy control individual. In the CFAP46-variant individual OP-64 II2, this band is not detectable, consistent with the abnormal immunofluorescence result. The weak band with a size of approximately 300 kDa correlates with a low amount of dysfunctional truncated CFAP46. DNAI2 (69 kDa) is detected as a loading control of protein extracts. **b, c)** Immunofluorescence microscopy analyses of respiratory epithelial cells are performed using antibodies directed against acetylated α -tubulin (green) and CFAP46 (red). Nuclei are stained with Hoechst 33342 (blue). Scale bars: 10 μ m. In healthy control cells, CFAP46 localises along the entire ciliary axoneme (**b**). In cells of CFAP46-variant individual OP-64 II2, CFAP46 is undetectable in the ciliary axoneme (**c**). DIC: differential interference contrast.

indicated a score of 7 (table 1). OI-102 II1 (*CFAP54*) reported chronic wet cough, recurrent pneumonia and bronchiectasis (table 1). The three *CFAP74*-variant individuals OP-3882 II1, OP-3882 II2 and OP-4027 II1 exhibited situs solitus and chronic respiratory disease. OP-3882 II1 had oligoasthenospermia. OP-3882 II2 did not have any children, but she has not requested any investigations regarding fertility in the past (supplementary table S2). In OP-3882 II2 and OP-4027 II1, the nNO production rates were 251.5 $\text{nL}\cdot\text{min}^{-1}$ and 504.6 $\text{nL}\cdot\text{min}^{-1}$, respectively (table 1) [12]. OP-3882 II1 and OP-3882 II2 had a PICADAR score of 2. OP-4027 II1 had a PICADAR score of 3 (table 1). The *CFAP221*-variant individual OP-2697 I2 reported chronic wet cough, bronchitis, sinusitis, otitis media and bronchiectasis. The nNO production rate was 28.9 $\text{nL}\cdot\text{min}^{-1}$ (table 1). The PICADAR for OP-2697 I2 was 4 (table 1).

Hydrocephalus was not reported in any of the here reported individuals.

Transmission electron microscopy

The ultrastructure of respiratory cilia was analysed by TEM in healthy control individuals and the affected individuals OP-64 II2 (*CFAP46*), OP-1245 II1 (*CFAP54*), OP-1822 II1 (*CFAP54*) and OP-2697 I2 (*CFAP221*). The axonemal cross-sections showed a normal ciliary 9+2 configuration without hallmark ultrastructural defects in all affected individuals (figure 3d and supplementary figure S2b) [23].

High-resolution immunofluorescence analyses and immunoblotting

To assess the integrity of the C1d projection, we performed high-resolution IF analyses in respiratory cilia from healthy control individuals and the *CFAP46*-, *CFAP54*-, *CFAP74*- and *CFAP221*-variant individuals (figures 4, 5 and 6). We used antibodies directed against CFAP46, after we confirmed the specificity by immunoblot analyses of extracts enriched for axonemal proteins. In the *CFAP46*-variant individual OP-64 II2, IF stainings revealed the absence of CFAP46 from the ciliary axonemes (figure 4). Moreover, CFAP46 was not detectable within the ciliary axonemes from the *CFAP54*-variant individuals OI-102 II1, OP-1245 II1, OP-1822 II1 and OP-4023 II1 (figure 5b–e). In addition, CFAP46 appeared reduced in the ciliary axonemes from the *CFAP74*-variant individuals OP-3882 II1, OP-3882 II2 and OP-4027 II1 (figure 5g–i). In contrast, the CFAP46 localisation was not affected in the *CFAP221*-variant individual OP-2697 I2 (figure 5j).

In extracts enriched for axonemal and cytoplasmic proteins from the *CFAP46*-variant individual OP-64 II2, the expected band of 303 kDa for CFAP46 was not detectable (figure 4a). In *CFAP54*- and *CFAP74*-variant individuals, CFAP46 was mislocalised in the cytoplasm and its axonemal assembly was impaired, as shown

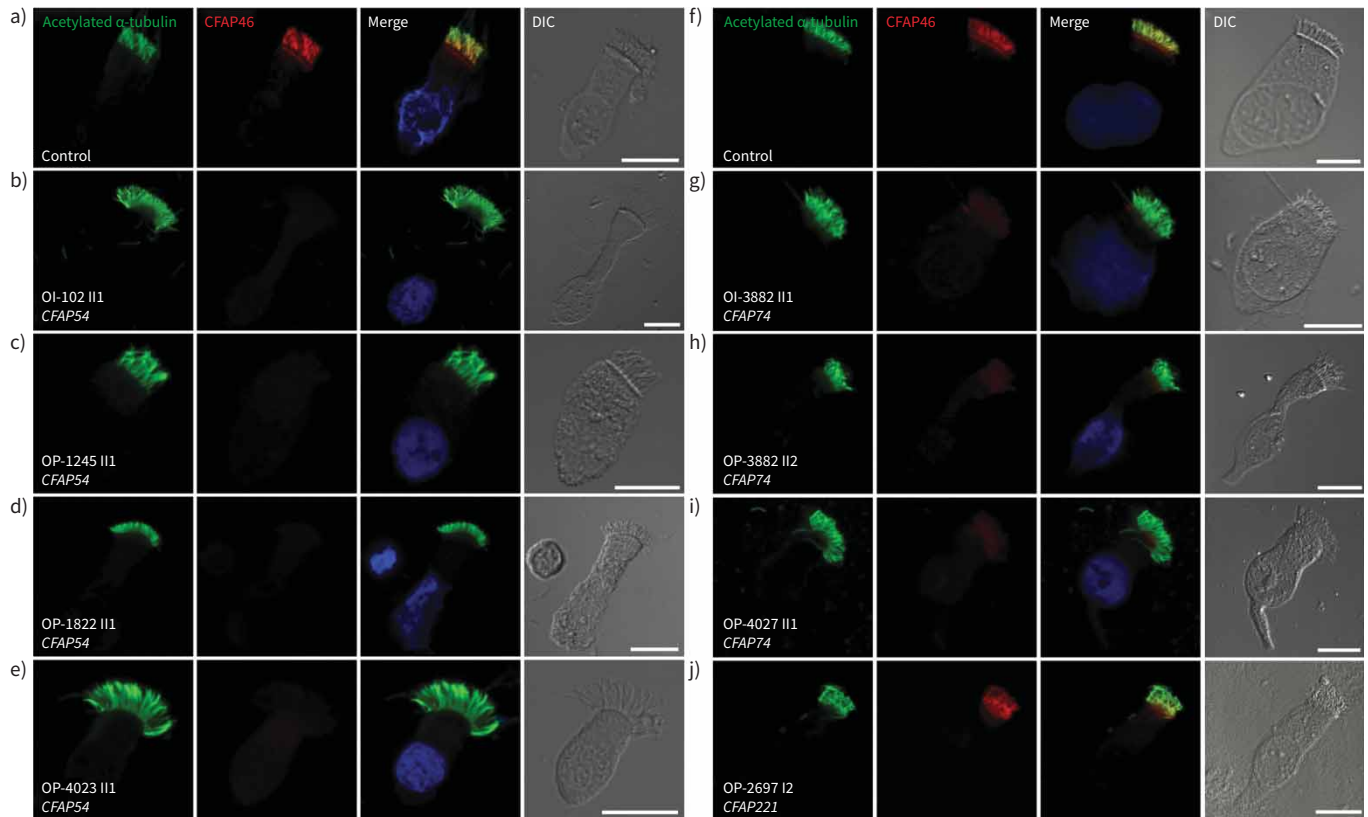


FIGURE 5 Axonemal localisation of CFAP46 in respiratory cilia from *CFAP54*-, *CFAP74*- and *CFAP221*-variant individuals. Immunofluorescence microscopy analyses of respiratory epithelial cells from healthy control individuals (a, f), *CFAP54*-variant individuals (b–e), *CFAP74*-variant individuals (g–i) and the *CFAP221*-variant individual (j). Cells are stained with antibodies directed against acetylated α -tubulin (green) and CFAP46 (red). Nuclei are stained with Hoechst 33342 (blue). Scale bars: 10 μ m. a, f) In cells from healthy control individuals, CFAP46 localises along the entire ciliary axoneme. b–e) CFAP46 is not detectable in the ciliary axoneme from the *CFAP54*-variant individuals OI-102 II1, OP-1245 II1, OP-1822 II1 and OP-4023 II1. g–i) CFAP46 appears to be reduced in the ciliary axoneme from the *CFAP74*-variant individuals OP-3882 II1, OP-3882 II2 and OP-4027 II1. j) In cells from the *CFAP221*-variant individual OP-2697 I2, the axonemal localisation of CFAP46 is not affected. DIC: differential interference contrast.

by anti-CFAP46 immunoblot analyses of extracts enriched for axonemal and cytoplasmic proteins (supplementary figure S5). Unfortunately, specific antibodies directed against CFAP54, CFAP74 and CFAP221 were not available.

IF stainings using antibodies targeting DNAH5, GAS8, RSPH9 (data not shown) and SPEF2 showed normal results consistent with a regular composition of the outer dynein arms, the nexin-dynein regulatory complexes, the radial spokes and the C1b projection (supplementary figure S6).

High-speed videomicroscopy analyses

To understand the functional deficits in affected individuals, we evaluated the ciliary beating in native respiratory epithelial cells by HSVMA at 25°C [13, 20]. In OP-64 II2 (*CFAP46*), OP-1245 II1 (*CFAP54*), OP-1822 II1 (*CFAP54*, reported externally), OP-4023 II1 (*CFAP54*, reported externally) and OP-2697 I2 (*CFAP221*), we detected CBFs within the normal range. In a few cells, we observed subtle changes, including a partially stiff, rotatory or uncoordinated ciliary beat pattern (CBP). However, those changes were also present in cells from healthy control individuals. In some individuals (OP-64 II2, OP-1245 II1, OP-1822 II1), we were able to perform HSVMA on ALI-cultured respiratory epithelial cells at 37°C after trypsinisation to separate cell clusters. They showed CBFs and CBPs similar to controls as well. The previously published *CFAP74*-variant individuals OP-3882 II1 and OP-3882 II2 displayed slightly reduced CBFs and we also found subtly changed CBPs in healthy control individuals (supplementary movie and table 1) [13]. For OP-4027 II1, normal ciliary beating was reported externally.

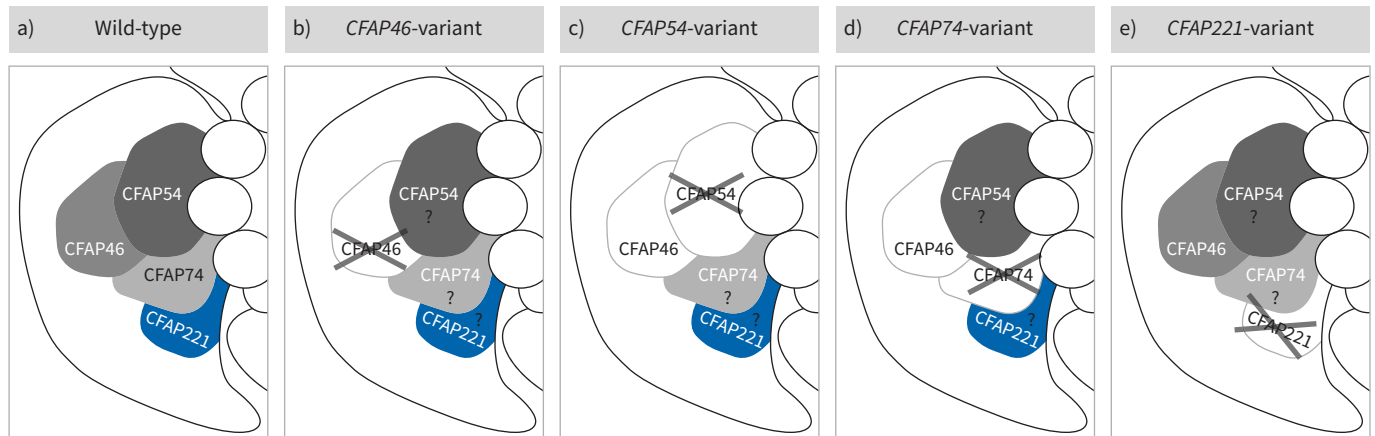


FIGURE 6 Model of the composition of the C1d projection in humans. **a)** Based on our immunofluorescence analyses using anti-CFAP46 antibodies, CFAP46, CFAP54 and CFAP74 form a heterotrimeric subcomplex (grey) within the human wild-type C1d projection. CFAP221 (blue) also belongs to the C1d projection but seems not to be directly involved in this heterotrimeric subcomplex, resembling findings in *Chlamydomonas reinhardtii* and indicating evolutionary conservation of the C1d projection. Our immunofluorescence analyses reveal the following. **b)** In a *CFAP46*-variant individual, CFAP46 is undetectable. **c)** In *CFAP54*-variant individuals, CFAP46 is not detectable, indicating that the CFAP46 assembly is dependent on functional CFAP54. **d)** In *CFAP74*-variant individuals, CFAP46 appears reduced within the ciliary axoneme, revealing that CFAP74 is involved in the assembly of CFAP46. **e)** In a *CFAP221*-variant individual, CFAP46 is not affected, which suggests a distal position of CFAP221 within the C1d projection. (Proteins directly affected by biallelic pathogenic variants are crossed out. Impaired protein assembly is illustrated by a white area with a grey border.)

In vitro ciliary transport assays

For the evaluation of the ciliary transport capacity, we performed *in vitro* ciliary transport assays in ALI-cultured respiratory epithelium from healthy control individuals, OP-64 II2 (*CFAP46*), OP-1245 III1 (*CFAP54*) and OP-1822 III1 (*CFAP54*) (figure 7 and supplementary figure S7). Interestingly, the mean CBFs within the cell layers from the affected individuals did not differ significantly from healthy controls ($p=0.62$, t-test). In contrast, the mean transport velocities of the fluorescent particles were significantly reduced in OP-64 II2 (37.6%), OP-1245 III1 (53.1%) and OP-1822 III1 (30.6%) ($p=0.00022$, t-test). In the *CFAP74*-variant individuals OP-3882 II1 and OP-3882 II2, we have previously reported reduced particle transport [13].

Discussion

In this study, we comprehensively characterised C1d-defective PCD in a total of nine individuals with pathogenic variants in *CFAP46*, *CFAP54*, *CFAP74* and *CFAP221* (table 1).

The function of the C1d projection is evolutionarily well conserved. *Cfap54*- and *Cfap221*-mutant mice exhibit mucus accumulation in the sinuses, hydrocephalus and male infertility, corresponding to a typical PCD phenotype in mice [24, 25]. In addition, *fap46*- and *fap74*-mutant *C. reinhardtii* strains showed impaired flagellar motility [26, 27]. In *C. reinhardtii*, it was demonstrated that FAP46, FAP54, FAP74 and FAP221 are C1d subunits [27]. Immunoprecipitation experiments in axonemal extracts further revealed that FAP46, FAP54 and FAP74 interact as a heterotrimeric subcomplex [26]. In immunoblot analyses of axonemal extracts, the absence of FAP46 severely reduced the levels of FAP54, FAP74 and FAP221. Whereas the absence of FAP74 caused reduced axonemal protein levels of FAP46 and FAP54, FAP221 was not detected. In the absence of both FAP46 and FAP74, only FAP54 remained detectable, with a reduced axonemal amount, suggesting a proximal position of FAP54 within the C1d projection [26]. Consistent with this, our findings suggest that CFAP46, CFAP54 and CFAP74 form a subcomplex in humans as well. As shown by anti-CFAP46 IF and immunoblot analyses, the physiological axonemal assembly of CFAP46 is dependent on functional CFAP54 and CFAP74 (figure 5b–i and supplementary figure S5). We expect CFAP54 at a proximal position within the C1d projection. In comparison, CFAP74 appears to be positioned slightly more distally, given that the axonemal CFAP46 assembly is impaired in the *CFAP74*-variant individuals but still detectable at low levels by IF microscopy. The regular assembly of CFAP46 in the *CFAP221*-variant individual OP-2697 II2 suggests a distal position of CFAP221, resembling findings in *C. reinhardtii* (figures 5 and 6). The lack of antibody availability targeting other C1d components such as CFAP54, CFAP74 and CFAP221 is a limitation of this study.

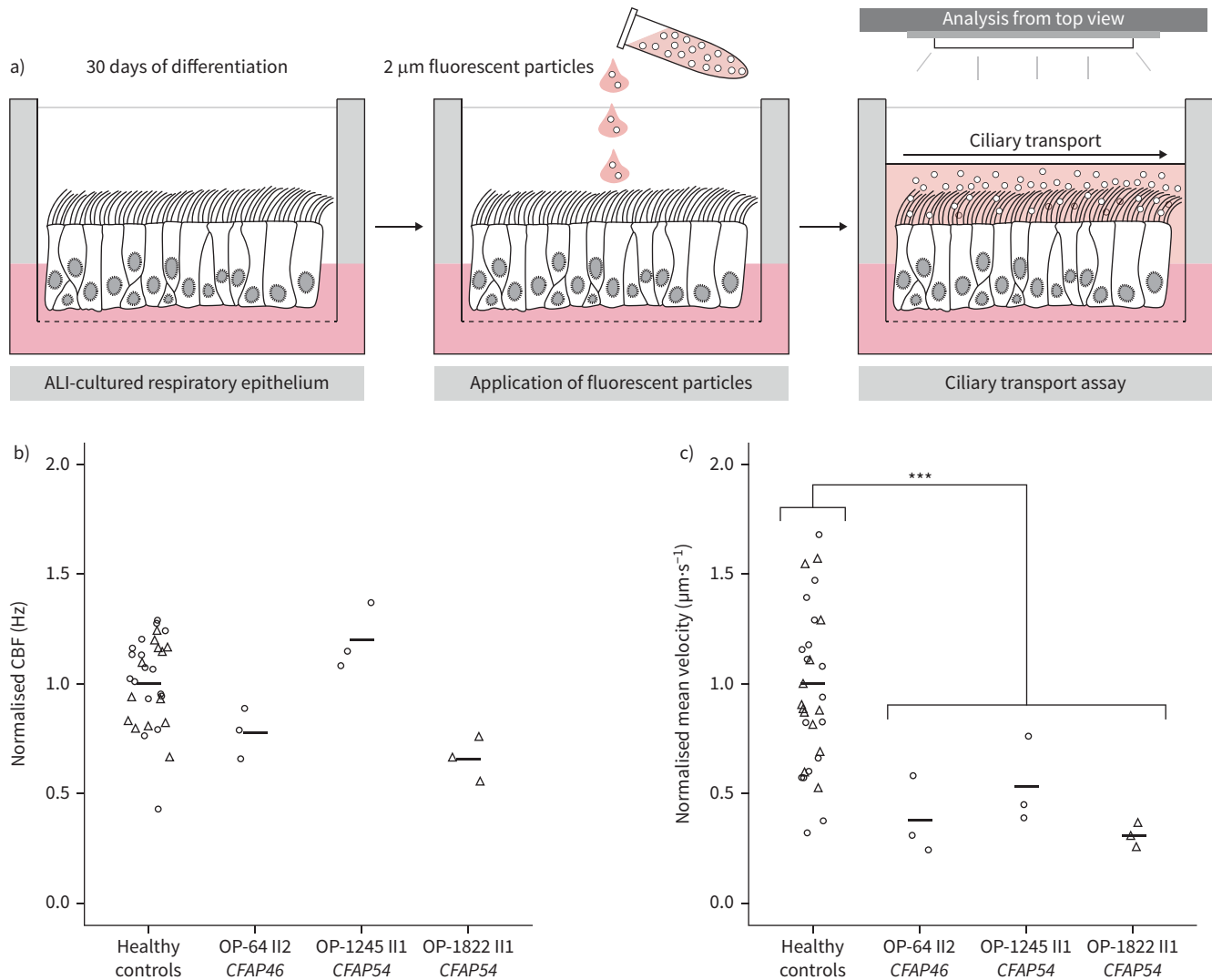


FIGURE 7 *In vitro* ciliary transport is impaired in *CFAP46*- and *CFAP54*-variant individuals. **a)** To assess the ciliary transport *in vitro*, respiratory epithelial cells from healthy control individuals and from *CFAP46*- and *CFAP54*-variant individuals were cultured at the air-liquid interface (ALI). After 30 days of differentiation, the ALI-cultured respiratory cell layers were used for ciliary transport assays, evaluating the transport of fluorescent particles by ciliary beating from the top view. **b)** The mean ciliary beat frequencies (CBFs) (indicated by the black bars) in OP-64 II2, OP-1245 II1 and OP-1822 II1 did not differ significantly from healthy controls ($p=0.62$, t-test). **c)** In contrast, the mean velocities of fluorescent particles were significantly reduced in the ALI-inserts from OP-64 II2 (37.6%), OP-1245 II1 (53.1%) and OP-1822 II1 (30.6%) ($p=0.00022$, t-test). Because two different microscope settings were used for the analysis, the data were normalised based on the healthy control pool (Nikon: triangles, Leica: circles). The exact values for CBF (Hz) and ciliary transport velocity ($\mu\text{m}\cdot\text{s}^{-1}$) are shown in supplementary figure S6. Significant differences are indicated. ***: $p<0.001$.

Moreover, we extensively characterised C1d-defective PCD according to the current ERS diagnostic guideline (supplementary figure S1) [7]. Notably, the PICADAR prediction tool is not adequate for reliable prediction of this PCD type. According to the work of BEHAN *et al.* [8], a PICADAR score of 2, 3 and 4 predicts PCD with a probability of 0.8%, 1.9% and 4.7%, respectively. Thus, PCD would have been considered unlikely in OP-64 II2 (*CFAP46*), OP-3882 II1 (*CFAP74*) and OP-3882 II2 (*CFAP74*) (PICADAR score of 2); OP-1245 II1 (*CFAP54*) and OP-4027 II1 (*CFAP54*) (PICADAR score of 3); and OP-2697 I2 (*CFAP221*) (PICADAR score of 4). A score of 6 for OP-1822 II1 (*CFAP54*) predicts PCD with a probability of 23.9%. Only OP-4023 II1 (*CFAP54*) reached a PICADAR of 7 (PCD prediction with a probability of 44.1%) [8]. To understand why PICADAR scores were low in these PCD individuals, we analysed the original publication reporting a mean PICADAR score in PCD-positive individuals of 7.9 ± 2.8 and in PCD-negative individuals of 3.8 ± 2.3 [8]. Interestingly, individuals were considered to be PCD-positive in case of a typical clinical history and at least two abnormal findings in TEM, CBP or nNO

production rate ($\leq 30 \text{ nL} \cdot \text{min}^{-1}$) [8]. Thus, there might be a bias for PCD individuals with abnormal ciliary ultrastructure to potentially exhibit higher PICADAR scores. Additionally, PICADAR is heavily reliant upon situs defects (4 points) and congenital heart defects (2 points), which substantially lowers the score in CA-defective PCD individuals.

Regarding symptoms, it is remarkable that neonatal respiratory distress and chronic ear symptoms are less common in this cohort (table 1), although these conditions are characteristic of most PCD types [1]. In C1d-defective PCD, chronic bronchitis, rhinosinusitis and recurrent pneumonia appear to be more characteristic. Future studies should address this point by studying larger cohorts of CA-defective PCD individuals, *e.g.* with disease-causing *HYDIN* variants. Currently, no general statement can be made on fertility (supplementary table S2). However, because male infertility was recently reported in *CFAP54*- and *CFAP74*-variant individuals [13, 14, 28], fertility tests should be recommended for C1d-defective PCD individuals.

nNO production rates with a cut-off of $77 \text{ nL} \cdot \text{min}^{-1}$ should identify PCD with a high degree of certainty [7]. However, in five of six individuals reported here, nNO levels were above this cut-off value (table 1). Normal nNO levels have also been described in other *CFAP54*- and *CFAP221*-variant individuals [12, 15]. Thus, nNO production rate measurements are not useful to detect C1d-defective PCD individuals. Interestingly, previous studies reporting low nNO levels in PCD individuals mainly used abnormal TEM and HSVMA findings as inclusion criteria [29, 30]. Thus, a bias towards lower nNO production rates in PCD with abnormal ultrastructure appears likely. In line with that, recent studies using genetic testing have confirmed that PCD with abnormal ultrastructure has indeed got lower nNO production rates [31, 32].

Here, HSVMA on native nasal brush biopsies and ALI-cultured respiratory epithelial cells showed findings similar to healthy controls, including minor changes such as slightly reduced CBFs or partially rotatory and stiff CBPs, representing the normal spectrum of ciliary beating within samples (supplementary video). Normal or only subtly changed ciliary beating was also described in other *CFAP54*- and *CFAP221*-variant individuals [12, 15]. In addition, it is known that both native and ALI-cultured cells may exhibit dyskinetic changes due to recent infections or cell disruption after sampling and processing [33–36]. Therefore, HSVMA is unable to distinguish between unaffected and C1d-defective PCD individuals.

TEM has been the diagnostic gold standard in the past (supplementary figure S1). However, because C1d-defective PCD individuals exhibit normal ciliary ultrastructure in respiratory epithelial cells (figure 3), TEM is unable to diagnose this PCD type. This applies to CA defects in general [9–13]. Future studies should address whether the interpretation of the HSVMA using formal waveform analysis (or artificial intelligence (AI)) and TEM including electron microscopy tomography using image analysis and AI may be able to resolve subtle differences not detected using standard visualisation.

As shown, C1d-defective PCD is particularly difficult to diagnose and remains easily overlooked. The late diagnosis in adulthood of most affected individuals underlines this (table 1) [14, 15]. Therefore, a different diagnostic approach is useful.

Genetic testing is part of the current ERS guideline but it is recommended as a third step (supplementary figure S1). Meanwhile, the less frequent use of genetic testing is especially known to contribute to the underdiagnosis of PCD [37], of which C1d-defective PCD might be an example. Interestingly, the diagnostic guideline of the American Thoracic Society recommends the early use of genetic testing subsequent to nNO measurements, considering the limitations of nNO measurements and the higher reliability of genetic testing [38]. Here, we report two novel PCD genes (*CFAP46* and *CFAP54*) aiding genetic diagnosis in PCD. However, it must be assumed that several PCD genes are still unidentified, highlighting the importance of further gene discovery in future studies.

IF microscopy is suitable for evaluating the pathogenicity of genetic variants or analysing the ciliary integrity in case of defects not assessable by TEM [7, 11, 39, 40]. We evaluated the integrity of the C1d projection using antibodies targeting *CFAP46*, which might be of particular interest if variants of unclear significance are detected. Because we only reported pathogenic variants here, IF microscopy was not necessary to establish the diagnosis. Owing to the rarity of C1d-defective PCD, IF microscopy is not a cost-effective screening method for this PCD type.

Recently, we introduced *in vitro* ciliary transport assays analysing the ciliary transport of fluorescent nanoparticles on ALI-cultured respiratory epithelium [17, 19]. We believe that this method has great potential to become an objective diagnostic method in specialised centres. Because it is time consuming and expensive, it is more likely to be used for novel and difficult to diagnose defects and might be applied

in selected cases. It is remarkable that the *in vitro* ciliary transport capacity is impaired despite normal HSVMA. Studies on model organisms might provide an explanation: in *C. reinhardtii*, the C1d projection is involved in the Ca²⁺-mediated coordination of flagellar beating [26, 27]. In mammals, this seems to apply less to the individual respiratory epithelial cell, but rather to the ciliary beat coordination of larger cell groups. Accordingly, in *Cfap54*-mutant mice, the tracheal CBF was reduced by only ~14.2%, but the ciliary flow rate on tracheal epithelium by ~46.9% [24]. CBP abnormalities were not described. Such larger cell groups cannot be fully analysed by HSVMA so potential abnormalities might remain undetected. In comparison, *in vitro* ciliary transport assays are suitable for this purpose because they analyse complete cell layers.

In summary, we report pathogenic variants in the novel PCD genes *CFAP46* and *CFAP54* and in the known PCD gene *CFAP221*, and we further analysed individuals with pathogenic variants in *CFAP74*. Our findings demonstrate that the diagnostic approach currently recommended by the ERS diagnostic guideline is not appropriate to detect C1d-defective PCD. To aid in identifying those PCD types, genetic testing should be prioritised in future guidelines, which is of particular interest as a new guideline is currently being developed.

Acknowledgements: We thank the PCD-affected individuals and their families for participation. We also gratefully acknowledge the German PCD support group “Kartagener Syndrom und Primäre Ciliäre Dyskinesie e.V.” and all referring physicians, especially Andrea Kessel from the Department of Pediatric Pneumology and Allergology, University Children’s Hospital Giessen and Marburg, Germany. For technical and organisational assistance, we thank M. Herting, L. Schwiddessen, S. Sivalingam, H. Book, H. Schmidt, B. Shin, S. Helms, M. Tekaas, F.-J. Seesing and A. Borgscheiper (Department of General Pediatrics, University Children’s Hospital Muenster, Muenster, Germany).

Ethics statement: This research project was approved by the Ethics Committee of the Medical Association of Westphalia-Lippe and the University of Muenster (reference number: 2015-104-f-S). Signed and informed consent was obtained from participating individuals, legal guardians and/or relatives by protocols approved by the Institutional Ethics Review Board of the University Muenster and collaborating institutions.

Conflict of interest: The authors have no potential conflicts of interest to disclose.

Support statement: This work was supported by grants from the Deutsche Forschungsgemeinschaft (OM6/7, OM6/8, OM6/10, OM6/14, OM6/16, CRU 326 (subprojects OM6/11 (H. Omran), RA3522/1 (J. Raidt), OL 450/3 (H. Olbrich)) and the Interdisziplinäres Zentrum für Klinische Forschung Muenster (Om2/009/12, Om2/015/16, Om2/010/20). Several authors are Healthcare Professionals in the European Reference Network ERN LUNG and/or members of the BEAT PCD clinical research collaboration (CRC) supported by the European Respiratory Society (ERS). Funding information for this article has been deposited with the Crossref Funder Registry.

References

- 1 Wallmeier J, Nielsen KG, Kuehni CE, *et al.* Motile ciliopathies. *Nat Rev Dis Primers* 2020; 6: 77.
- 2 Horani A, Ferkol TW. Understanding primary ciliary dyskinesia and other ciliopathies. *J Pediatr* 2021; 230: 15–22.
- 3 Hannah WB, Seifert BA, Truty R, *et al.* The global prevalence and ethnic heterogeneity of primary ciliary dyskinesia gene variants: a genetic database analysis. *Lancet Respir Med* 2022; 10: 459–468.
- 4 Ishikawa T. Axoneme structure from motile cilia. *Cold Spring Harb Perspect Biol* 2017; 9: a028076.
- 5 Samsel Z, Sekretarska J, Osinka A, *et al.* Central apparatus, the molecular kickstarter of ciliary and flagellar nanomachines. *Int J Mol Sci* 2021; 22: 3013.
- 6 Gui M, Wang X, Dutcher SK, *et al.* Ciliary central apparatus structure reveals mechanisms of microtubule patterning. *Nat Struct Mol Biol* 2022; 29: 483–492.
- 7 Lucas JS, Barbato A, Collins SA, *et al.* European Respiratory Society guidelines for the diagnosis of primary ciliary dyskinesia. *Eur Respir J* 2017; 49: 1601090.
- 8 Behan L, Dimitrov BD, Kuehni CE, *et al.* PICADAR: a diagnostic predictive tool for primary ciliary dyskinesia. *Eur Respir J* 2016; 47: 1103–1112.
- 9 Olbrich H, Schmidts M, Werner C, *et al.* Recessive *HYDIN* mutations cause primary ciliary dyskinesia without randomization of left-right body asymmetry. *Am J Hum Genet* 2012; 91: 672–684.
- 10 Edelbusch C, Cindrić S, Dougherty GW, *et al.* Mutation of serine/threonine protein kinase 36 (*STK36*) causes primary ciliary dyskinesia with a central pair defect. *Hum Mutat* 2017; 38: 964–969.
- 11 Cindrić S, Dougherty GW, Olbrich H, *et al.* *SPEF2*- and *HYDIN*-mutant cilia lack the central pair-associated protein *SPEF2*, aiding primary ciliary dyskinesia diagnostics. *Am J Respir Cell Mol Biol* 2020; 62: 382–396.

- 12 Bustamante-Marin XM, Shapiro A, Sears PR, *et al.* Identification of genetic variants in *CFAP221* as a cause of primary ciliary dyskinesia. *J Hum Genet* 2020; 65: 175–180.
- 13 Biebach L, Cindrić S, Koenig J, *et al.* Recessive mutations in *CFAP74* cause primary ciliary dyskinesia with normal ciliary ultrastructure. *Am J Respir Cell Mol Biol* 2022; 67: 409–413.
- 14 Sha Y, Wei X, Ding L, *et al.* Biallelic mutations of *CFAP74* may cause human primary ciliary dyskinesia and MMAF phenotype. *J Hum Genet* 2020; 65: 961–969.
- 15 Zhao X, Ge H, Xu W, *et al.* Lack of *CFAP54* causes primary ciliary dyskinesia in a mouse model and human patients. *Front Med* 2023; 17: 1236–1249.
- 16 Loges NT, Antony D, Maver A, *et al.* Recessive *DNAH9* loss-of-function mutations cause laterality defects and subtle respiratory ciliary-beating defects. *Am J Hum Genet* 2018; 103: 995–1008.
- 17 Wallmeier J, Frank D, Shoemark A, *et al.* *De novo* mutations in *FOXJ1* result in a motile ciliopathy with hydrocephalus and randomization of left/right body asymmetry. *Am J Hum Genet* 2019; 105: 1030–1039.
- 18 Richards S, Aziz N, Bale S, *et al.* Standards and guidelines for the interpretation of sequence variants: a joint consensus recommendation of the American College of Medical Genetics and Genomics and the Association for Molecular Pathology. *Genet Med* 2015; 17: 405–424.
- 19 Wallmeier J, Bracht D, Alsaif HS, *et al.* Mutations in *TP73* cause impaired mucociliary clearance and lissencephaly. *Am J Hum Genet* 2021; 108: 1318–1329.
- 20 Raidt J, Wallmeier J, Hjej R, *et al.* Ciliary beat pattern and frequency in genetic variants of primary ciliary dyskinesia. *Eur Respir J* 2014; 44: 1579–1588.
- 21 Shapiro AJ, Dell SD, Gaston B, *et al.* Nasal nitric oxide measurement in primary ciliary dyskinesia. A technical paper on standardized testing protocols. *Ann Am Thorac Soc* 2020; 17: e1–e12.
- 22 Omran H, Loges NT. Immunofluorescence staining of ciliated respiratory epithelial cells. *Methods Cell Biol* 2009; 91: 123–133.
- 23 Shoemark A, Boon M, Brochhausen C, *et al.* International consensus guideline for reporting transmission electron microscopy results in the diagnosis of primary ciliary dyskinesia (BEAT PCD TEM Criteria). *Eur Respir J* 2020; 55: 1900725.
- 24 McKenzie CW, Craig B, Kroeger TV, *et al.* *CFAP54* is required for proper ciliary motility and assembly of the central pair apparatus in mice. *Mol Biol Cell* 2015; 26: 3140–3149.
- 25 Lee L, Campagna DR, Pinkus JL, *et al.* Primary ciliary dyskinesia in mice lacking the novel ciliary protein *Pcdp1*. *Mol Cell Biol* 2008; 28: 949–957.
- 26 Brown JM, Dipetrillo CG, Smith EF, *et al.* A *FAP46* mutant provides new insights into the function and assembly of the C1d complex of the ciliary central apparatus. *J Cell Sci* 2012; 125: 3904–3913.
- 27 Dipetrillo CG, Smith EF. *Pcdp1* is a central apparatus protein that binds Ca^{2+} -calmodulin and regulates ciliary motility. *J Cell Biol* 2010; 189: 601–612.
- 28 Tian S, Tu C, He X, *et al.* Biallelic mutations in *CFAP54* cause male infertility with severe MMAF and NOA. *J Med Genet* 2023; 60: 827–834.
- 29 Marthin JK, Nielsen KG. Choice of nasal nitric oxide technique as first-line test for primary ciliary dyskinesia. *Eur Respir J* 2011; 37: 559–565.
- 30 Marthin JK, Nielsen KG. Hand-held tidal breathing nasal nitric oxide measurement – a promising targeted case-finding tool for the diagnosis of primary ciliary dyskinesia. *PLoS One* 2013; 8: e57262.
- 31 Legendre M, Thouvenin G, Taytard J, *et al.* High nasal nitric oxide, cilia analyses, and genotypes in a retrospective cohort of children with primary ciliary dyskinesia. *Ann Am Thorac Soc* 2022; 19: 1704–1712.
- 32 Raidt J, Krenz H, Tebbe J, *et al.* Limitations of nasal nitric oxide measurement for diagnosis of primary ciliary dyskinesia with normal ultrastructure. *Ann Am Thorac Soc* 2022; 19: 1275–1284.
- 33 Chilvers MA, Rutman A, O’Callaghan C. Functional analysis of cilia and ciliated epithelial ultrastructure in healthy children and young adults. *Thorax* 2003; 58: 333–338.
- 34 Thomas B, Rutman A, O’Callaghan C. Disrupted ciliated epithelium shows slower ciliary beat frequency and increased dyskinesia. *Eur Respir J* 2009; 34: 401–404.
- 35 Hirst RA, Rutman A, Williams G, *et al.* Ciliated air–liquid cultures as an aid to diagnostic testing of primary ciliary dyskinesia. *Chest* 2010; 138: 1441–1447.
- 36 Hirst RA, Jackson CL, Coles JL, *et al.* Culture of primary ciliary dyskinesia epithelial cells at air–liquid interface can alter ciliary phenotype but remains a robust and informative diagnostic aid. *PLoS One* 2014; 9: e89675.
- 37 Shoemark A, Griffin H, Wheway G, *et al.* Genome sequencing reveals underdiagnosis of primary ciliary dyskinesia in bronchiectasis. *Eur Respir J* 2022; 60: 2200176.
- 38 Shapiro AJ, Davis SD, Polineni D, *et al.* Diagnosis of primary ciliary dyskinesia. An official American Thoracic Society clinical practice guideline. *Am J Respir Crit Care Med* 2018; 197: e24–e39.
- 39 Frommer A, Hjej R, Loges NT, *et al.* Immunofluorescence analysis and diagnosis of primary ciliary dyskinesia with radial spoke defects. *Am J Respir Cell Mol Biol* 2015; 53: 563–573.
- 40 Goutaki M, Shoemark A. Diagnosis of primary ciliary dyskinesia. *Clin Chest Med* 2022; 43: 127–140.